Modelling the influence of carbides on tool wear

J. Lorentzon*, N. Järvstråt

Department of Technology, Mathematics and Computer Science,
University West, Trollhättan, Sweden
* Corresponding author: E-mail address: john.lorentzon@hv.se

ABSTRACT

Purpose: The complex mechanisms of tool wear in metal cutting have not been possible to investigate in detail by the experimental methods traditionally employed. However, as a result of both the continuous development of numerical methods, such as the Finite Element Method (FEM) and the development of ever more powerful computers, the evaluation of the chip formation process and the evolution of tool wear is now possible.

Design/methodology/approach: : In the work presented in this paper, numerical methods are employed to study the effect of a single embedded hard carbide particle on tool wear and tool tip deformation. An important advantage of this approach is that particle size and position can easily be changed, thus making it possible to investigate the influence of these parameters on tool wear.

Findings: The results reveal that the position, and in particular the size of carbide particles, have a dramatic impact on tool wear. In particular, particles larger than a certain size (about 5μm) cause significant plastic deformation of the tool tip, when passing in sufficient proximity.

Research limitations/implications: An effort has been made to obtain the corrected version of the stability polynomial, the corresponding stability region and the range of Re(z) for the RK-Butcher algorithm.

Originality/value: The present article sheds some light on different numerical integration algorithms involved in robot arm model problem.

Keywords: Carbides; Tool wear; Finite Element Method; Inconel 718; Machining; Micro-structure; Simulation; Chip formation; Tool plastic deformation; Computational materials science

Reference to this paper should be given in the following way:

J. Lorentzon, N. Järvstråt, Modelling the influence of carbides on tool wear, Archives of Computational Materials Science and Surface Engineering 1/1 (2009) 29-37.

ENGINEERING MATERIALS PROPERTIES

1. Introduction

Significant efforts have been made to understand the nature of tool wear in machining processes. However, even though the complexity of conditions in the cutting zone mean that the nature of tool wear is still not sufficiently understood, it is nevertheless accepted that tool wear is induced by adhesion, abrasion, diffusion and/or oxidation. Although commonly any combination of these may be of importance, in any given set of conditions, it is usually the case that a single, or indeed a limited number of these mechanisms, exerts a dominant influence. At present, experimentation is the main method used for investigating wear processes. However, continuous development of numerical methods such as the Finite Element Method (FEM) together with the availability of more powerful computers enables simulation of complicated problems such as cutting processes.

FEM has proved to be an effective technique for analysing chip formation processes and predicting process variables such as temperatures, forces, stresses etc. Therefore, the use of simulations has increased considerably during the last decade, with the coupled thermo-mechanical simulation of the chip formation process being a method used by many researchers, such as [2,10,15,22]. Recently predictions of the evolution of tool wear have been performed by implementing a wear rate equation, such as Usui's equation, in FE software. In such cases the wear rate has been calculated from predicted cutting variables whilst the tool geometry is updated by moving the nodes of the tool. The method has been used by [8,21,22] showing reasonably good accuracy and can currently be regarded as the state-of-the-art in the modelling of machining processes.

In most FE models of chip formation processes, the work material is treated as homogenous, with micro-structural effects, such as grain size and carbides, being disregarded. However, Chuzhoy *et. al.,* [3] have developed an FE-model for the machining of ductile iron that included microstructural components such as pearlite, ferrite and graphite particles [3,4,5]. This method has also been used by Simoneau, and Elbestawi, [18] where an excellent chip shape correlation between simulation and experiment was achieved. As far as the authors are aware, the microstructure has, to date, not however been implemented in an FE wear model, despite the common assumption that the microstructure has a significant influence on the wear rate of the tool. Therefore, when predicting tool wear in machining it is important that the microstructure should be included. Further, the inclusion of carbides and other hard inclusions is of particular importance, since these are believed to be the dominating causes of abrasive wear. Indeed, this was identified as being the main wear mechanism by Focke *et al.,* [9] when he examined tungsten-carbide tools after machining Inconel 718, a precipitation-hardened nickel-based alloy. As carbides embedded in the workpiece material are considered to be one of the main sources of tool wear in machining of Inconel 718, it is of great importance to incorporate this in a model of tool wear, especially as our current understanding of what happens when carbides collide with the tool is rather limited. The microstructure of Inconel 718 can be seen in Figure 1 [26] showing a block-shaped titanium-carbide of about 10 μm in size.
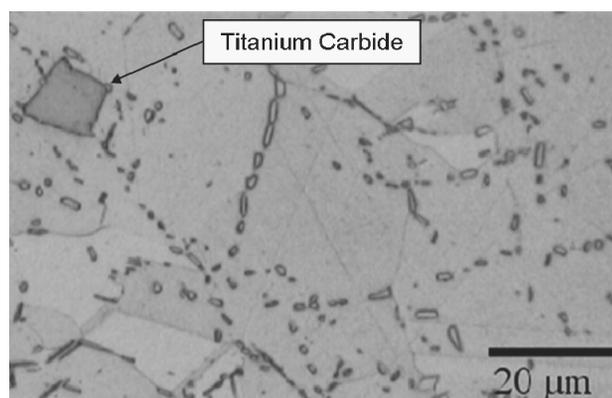
Fig. 1. Optical micrograph from [26] showing an embedded Titanium carbide particle in a matrix of Inconel 718

The aim of the work presented in this paper is to develop our understanding of the influence of hard particles such as carbides on wear mechanisms during machining. To capture these phenomena, a hard particle embedded in a softer Inconel 718 work material has been modelled at the point at which it "collides" with an uncoated cemented carbide tool, worn to a representative state. The wear is estimated using Usui's wear rate model [11,12,20] previously implemented in MSC.Marc [14].

2. Tool wear model

The tool wear model consists of a FE chip formation model and a wear model implemented as subroutines calculating the wear rate at contact points and modifying the tool geometry accordingly.

2.1. Chip formation model

The FE chip formation model was created using the commercial software MSC. Marc, which uses an updated Lagrange formulation. This means that the material is attached to the mesh, but with periodic remeshing to avoid element distortion. The cutting process requires a coupled thermo mechanical analysis, because mechanical work is converted into heat, causing thermal strains and influencing the material properties. Two types of thermal assumptions are commonly used for the simulation of mechanical cutting, namely adiabatic heating, and fully coupled thermal-mechanical calculations. In this work a coupled, staggered, model was used. This means that for each time step, set to 1μs in all of the analyses, the heat transfer analysis is conducted first, and thereafter the stress analysis. Quasi-static analyses were used, which means that the heat analysis is transient while the mechanical analysis is static with inertia forces neglected.

The FE chip formation model consists of a deformable tool, workpiece and carbide particle. As a slight simplification, the carbide (c.f. Figure 1) was modelled as quadratic, embedded in the work piece according to Figure 2. The contact condition between the carbide and the tool was set as fully bonded, with no slip or debonding allowed. The tool is modeled with elastoplastic properties and is constrained in x and y-directions at the top and left edges in Figure 2.
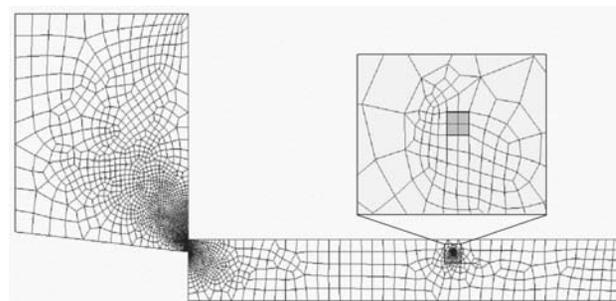
Fig. 2. Simulation model mesh for the 10 μm particle at 98 μm depth. The four grey elements constitute the carbide

Dimensions

The dimensions of the workpiece used in the simulation model are: 5 mm in length by 0.5 mm in height. The tool used in the simulation model is 2 mm long and 2 mm high. The cutting edge radius was 16 µm, the clearance angle 6° and the rake angle 0°; the feed was 0.1 mm and the cutting speed was 0.75 m/s. The carbide size modelled was 5, 10 and 15 µm. The carbide size in forged Inconel718 is in the 3 and 10 µm range [26].

Mesh

The mesh of the workpiece is shown in Figure 2. The remeshing technique used was the "advancing front quad". This mesh generator starts by creating elements along the boundary of the given outline. Mesh creation continues inward until the entire region has been meshed. The number of elements used was about 6000, with the minimum element size set to be 2 µm. As seen in Figure 2, a finer mesh was used around the tool tip, where the material separates. The element net was also chosen to fit the carbide, which was meshed with element size 5 µm. The tool was meshed with 5000 elements with a minimum element size of 2 µm.

Material properties

Generally, the strain magnitude, the strain rate, and the temperature each have a strong influence on the material flow stress. Thus, it is necessary to capture these dependencies in the material model used in order to correctly predict the chip formation. Here, neglecting a slight (about 10 % between 1/s and 10^4/s at room temperature according to [1] and nearly zero between 10^2/s and 10^5/s at 300° C according to Fang [6], strain rate dependency, a rate-independent piecewise linear plasticity model was used. Instead, the flow stress curve for high strain rate (10^4/s) was used, see Figure 3. The temperature trend of the flow stress is taken from [17]. The other work-piece material properties [24] used are illustrated in Figure 4.
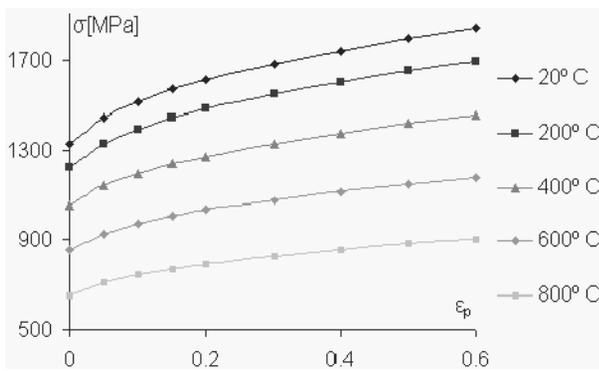
Fig. 3. Flow stress curves (Curve at room temperature [1] and temperature trend [17]

Because of its small size, the titanium-carbide particle is considered to be a single crystal. The material properties were considered independently of temperature, and are set out in Table 1 [16,25].

The material properties of the uncoated cemented carbide tool were considered independently of temperature, and are set out in Table 2 [15,19,22,23].
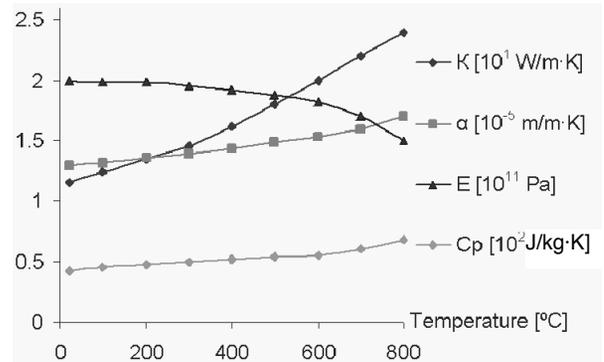
Fig. 4. Young's modulus, E, specific heat capacity, Cp, thermal conductivity, K, poisons ratio, ν, and thermal expansion, α, from [24]

Table 1.
Titanium carbide properties[1] [16]

Density [kg/m^3]	4900 [2]
Young's modulus [GPa]	497 [2]
Poisson's ratio	0.188 [1]
Yield limit [MPa]	20000 [2]
Thermal expansion	$6.4 \cdot 10^{-6}$ [2]
Specific heat capacity [J/kg·K]	700 [1]
Thermal conductivity [W/m·K]	330 [2]

Table 2.
Tool material properties for the cemented carbides [15,19,22,23]

Density [kg/m^3]	11900 [3]
Young's modulus [GPa]	630 [2]
Poisson's ratio	0.26 [1]
Yield limit [MPa]	4250 [2]
Thermal expansion	$5.4 \cdot 10^{-6}$ [1]
Specific heat capacity [J/kg·K]	334 [3]
Thermal conductivity [W/m·K]	100 [2]

Friction model

Two regions can be identified on the rake face of the tool; a sliding region and a sticking region [19]. Whilst in the sliding region a Coulomb friction model can be used, this is not however considered appropriate for the sticking region [19]. Thus, in order to employ the same friction model throughout, a shear friction model was used in this work. This model states that the friction force is a fraction of the equivalent stress, see Equation 1.

$$\sigma_{fr} = m \cdot \frac{\sigma_{eqv}}{\sqrt{3}} \tag{1}$$

The friction coefficient was calibrated to correlate within 5 % on the simulated and measured feed force, giving a friction coefficient m = 1.1.

Heat generation

In the machining process heat is generated by friction and plastic deformation. The rate of specific volumetric flux due to plastic work is given by Equation 2.

$$\dot{q} = \frac{f \cdot \dot{W}_p}{\rho} \qquad (2)$$

where $\dot{W}_p$ is the rate of plastic work, ρ is the density and f is the fraction of plastic work converted into heat, which is set to 1. Strictly speaking, this is not correct because although some plastic work is stored in the material, the relative fraction stored is however unknown [10], and since the deformations are so large, the fraction of plastic work stored is neglected.

The rate of heat generated due to friction is given by Equation 3.

$$\dot{Q} = F_{fr} \cdot v_r \qquad (3)$$

where F_{fr} is the friction force and v_r is the relative sliding speed. The heat generated due to friction is equally distributed into the two contact bodies. This heat is transferred from the workpiece, due to convection to the environment and conduction to the tool. Radiation has been neglected. The heat transfer coefficient at the contact between the tool and the workpiece was set to 1000 kW/m^{2}K which, according to [7] permits a satisfactory agreement between numerical data and the experimental evidence, although it should be noted that this was utilized for another material combination. The temperature at the outer boundary of the tool and the workpiece was fixed at room temperature.

2.2. Wear model

Usui's [11,12,20] empirical wear rate model (Equation 4) was used in this work. In this model, the wear rate is a function of contact pressure, σ_n, relative velocity, v_{rel} and absolute temperature, T. The constants in the empirical wear model were determined by [14] through calibrating machining simulations with measured wear rates for the same conditions. Initially, tool wear machining tests for the selected material were performed. Thereafter, FE simulations were conducted under the same conditions and, finally, the constants of the wear rate model were calculated by regression analysis, giving the constants A = 1.82·10^{-12} and B = 8900.

$$\frac{dw}{dt} = A \cdot \sigma_n \cdot v_{rel} \cdot e^{-\frac{B}{T}} \qquad (4)$$

3. Analysis stages

In a turning operation, a stationary condition with respect to temperature and forces is generally achieved within seconds following the penetration of the workpiece by the tool. Therefore, the initial chip formation can be neglected in predictions of the progress of tool wear. Instead, tool wear predictions are made on stationary chip formation conditions, with the first step in tool wear predictions being the calculation of the stationary chip condition. Since the tool geometry rapidly approaches a worn state, tool wear is calculated in the second step, thus allowing the carbide particle to interact with the worn tool geometry in the final step.

3.1. Chip formation

Generally it is not possible to obtain stationary conditions in FE chip formation simulations using the Lagrangian method, since the whole object on which chip formation simulation is performed must be present as a meshed object at the very outset of the simulation. This has the consequence that a transient analysis designed to reach steady-state conditions would be computationally prohibitive [10] without acceleration attaining a steady state. Fortunately, by lowering the specific capacity of the tool, it is possible to achieve a considerable rate of acceleration, see Figure 5.
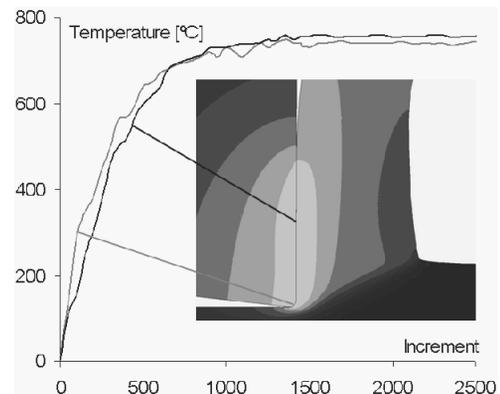
Fig. 5. Temperature histories for two nodes in the tool reaching stationary conditions with respect to temperature after a 1500 increment, corresponding to 1500 micro seconds

The reason for this is that a lowering of the specific heat capacity has the same effect as taking a larger time step, as compared to a mechanical step, in the thermal calculations as can be seen in Equation 5. Note that the left hand side of the equation vanishes at steady state, while an increased C_p increases the rate of change and thus accelerates before reaching the steady state condition.

$$\rho \cdot C_p \frac{\partial T}{\partial t} = k\left(\frac{\partial^2 T}{\partial x^2} + \frac{\partial^2 T}{\partial y^2} + \frac{\partial^2 T}{\partial z^2}\right) \qquad (5)$$

Here, T is the temperature, k is the thermal conductivity, ρ is the density, and C_p is the specific heat capacity.

3.2. Tool wear

The tool wear model consists of a FE chip formation model and a wear model implemented as subroutines with calculations of the wear rate made at contact points and thereafter subsequent modifications of the tool geometry. The wear rate is calculated using Usui's empirical wear model for every node of the tool that is in contact with the base material. In order to do this, the temperature, relative velocity, and contact stress are calculated in the FE chip formation simulation for all nodes of the tool that are in contact with the workpiece in the process. The calculated values are then employed by a user subroutine to calculate the wear rate, see Figure 6. Based on the calculated wear rate, the geometry of the tool is updated by moving specific nodes of the tool in the FE simulation, see [22] for a more comprehensive

description. The direction of the movement of a node is based on the direction of the contact pressure at that node. After moving the node, all integration point data is mapped to the new integration point positions and the chip formation simulation continues, with the tool penetrating through the work material. Since the elements become distorted as the geometry of the tool is updated, the tool mesh is automatically remeshed using the "advancing front quad" remeshing technique to compensate for this.
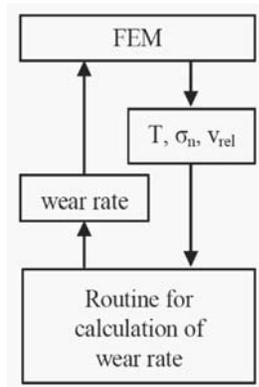
Fig. 6. Schematic illustration of the system for tool wear calculations

The wear calculations are started at increment 1800, see Figure 5, with the tool at a steady state with respect to both force and temperature. The wear calculation is subdivided into 800 increments, each with tool geometry updating. If fewer increments were to be used, convergence problems and numerical errors would occur, whereas if a greater number of increments had been included, the computation time would increase unnecessarily. The wear calculation corresponds to approximately 15 seconds of dry machining, resulting in 55 µm flank wear land and 4 µm crater depth. Hence, the wear process is accelerated by about 20 000 times in the simulation model.

3.3. Carbide collision

Using the worn tool geometry as calculated in the previous calculation step, a simulation of one carbide particle passing the tool as it penetrates through the work material, is performed. The tool geometry is not updated in this load step, and the heat capacity in the tool is set to a nominal value for the simulation of the carbide embedded in the work material as it approaches and passes the tool. This is carried out for quadratic carbides positioned at several different depths below the workpiece surface as set out in Table 3. The positions are selected in such a way that they include both simulations of carbides following the chip up along the tool rake face, as well as those carbides that pass below the tool tip. The path for carbides with the central point positioned at 96 and 97 µm below the workpiece surface is shown in Figure 7. The carbide positioned at 97 µm below the workpiece surface passes below the tool tip, while the carbide positioned 1 µm higher up follows the chip along the rake face. In addition to these measurements, the effect of carbide size is also investigated for carbide positions where the carbide passes just below the tool.

Table 3.
Carbide sizes and positions used in the simulations

Depth position [µm]	Carbide size [µm]
101	10
99	10
97	10
96	10
94	10
96	15
98	5
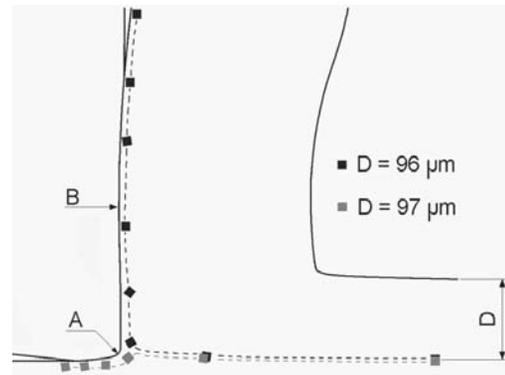
Fig. 7. Path for carbides at depths of 96 and 97 µm below the workpiece surface, where the first position represents the start of the carbide collision analysis step. A and B mark the positions where the crater and the flank wear respectively are presented

4. Results and discussion

In this chapter the impact of carbides embedded in the workpiece on tool wear, stresses and plastic deformation of the tool are presented. Depending on where the carbide is located, different scenarios will arise; in the first part of this chapter the flank face is of interest as the carbide passes below the tool, while the rake face is brought into focus in the latter part as the path of the carbide is deflected upwards in the chip (c.f. Figure 7).

4.1. Flank wear

Figure 8 shows the stresses in the tool when a quadratic carbide with a dimension of 10 µm passes through the primary and tertiary shear zones. The carbide's start position is 97 µm below the workpiece surface, measured from the centre of the carbide. The carbide rotates as it passes the shear zones and the stress level in the tool increases above the yield limit, causing plastic deformation of the tool. This is seen clearly in Figure 8 (c and d), where the tool has been significantly deformed. Figure 8 (e and f) shows that the surface near the carbide becomes uneven, thus decreasing the quality of the machined surface. An interesting observation outlined in Figure 8 is that the carbide never actually comes into contact with the tool, because it is always surrounded by material. We believe this to be a real physical effect, and not an artefact of the simulations, although more thorough investigations need to be

performed in order to achieve verification. When considering this effect, one should recall that the material around the tool tip experiences extremely high hydrostatic pressure, which counteracts crack initiation and growth in the material surrounding the carbide. Further, it should be noted that the stresses in the carbide particle are well below yield as it passes through the shear zone due to the much higher yield limit, compared to the base metal, in the carbide.

a)

b)

c)

d)

e)

f)
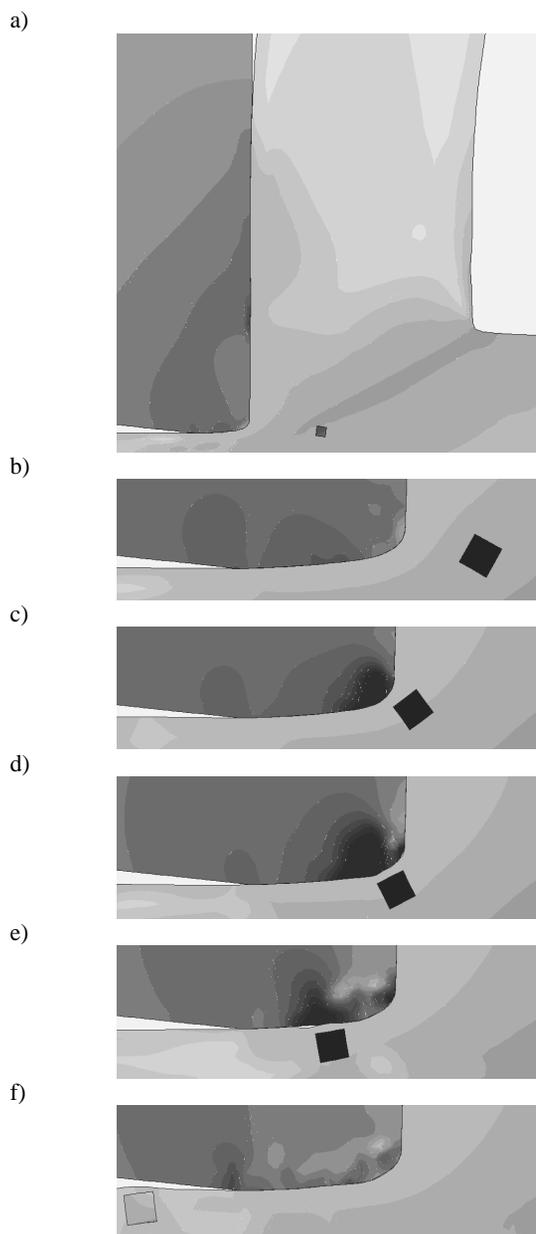
Fig. 8. Equivalent stresses in the tool as a carbide passes below the tool at different points in time (measured from the start of the carbide collusion analysis, c.f. Figure 7); (a) 600 µs, (b) 700 µs, (c) 750 µs, (d) 775 µs , (e) 800 µs, (f) 900 µs. The size of the carbide is 10 µm with a start position 97 µm below the workpiece surface measured from the centre point of the carbide

Wear

In Figure 9, tool wear is presented for point A in Figure 7 as the carbide with a dimension of 10 µm at different depths passes the tool tip. The tool wear is calculated using Usui's wear equation, see Equation (4). The Figure shows that the effect of tool wear caused by the carbide is dependent on the position of the carbide. The maximum impact of the carbide on the tool wear rate is found when the carbide passes as close as possible below the tool. At 97 µm depth, which is close to this critical point, one carbide particle causes $32 \cdot 10^{-12}$ m extra tool wear, or about the equivalent to the wear caused by machining an extra length of 100 µm. The extra wear caused by the particle decreases with the carbide's distance below the critical point, though this dependence of distance is moderate, with ¾ of the wear retained at a depth of 99 µm, and half of the wear at 97 µm retained at a carbide depth position of 101 µm. The increase in tool wear is mainly due to an increase in pressure acting on the tool, with the temperature remaining essentially unaffected by the brief passage of one particle, whilst the relative velocity between the tool and the workpiece changes only slightly.
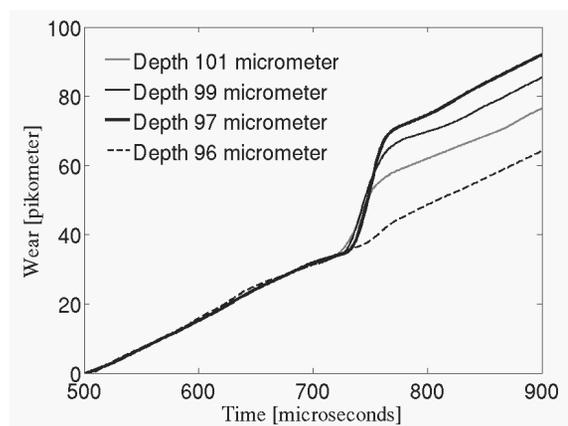
Fig. 9. Wear measured in point A, see Figure 7, when carbides with dimension 10 µm at different depths pass the tool tip
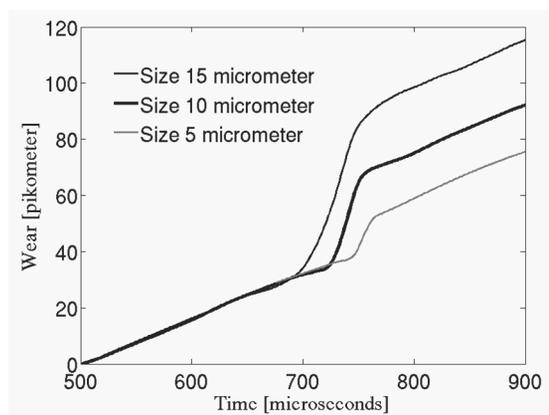
Fig. 10. Wear measured in point A, see Figure 7, for different carbide sizes at depth 97 µm

In Figure 10 tool wear is presented for point A in Figure 7 as carbides with dimensions of 5, 10 and 15 µm pass the tool tip. It can be seen that the influence of carbide size is slightly stronger than a linear progression, with a 15 µm particle achieving 60% more wear than a 10 µm particle, while a 5 µm particle achieves about one third of the wear of a 10 µm particle.

Plastic deformation

Figure 11 shows the tool-tip plastic displacement (point A in Figure 7) for different depth positions of a 10 µm particle. The carbide positioned 97 µm below the workpiece surface results in as much as 0.85 µm plastic deflection of the tool tip. If the carbide is instead positioned 99 µm below the workpiece surface it will give a 0.15 µm plastic deflection of the tool tip, while a carbide positioned 101 µm below the workpiece surface will achieve no plastic deformation of the tool. Further, no plastic deformation of the tool is noticed if the carbide is positioned 96 µm below the workpiece surface, as the carbide is then deflected upwards in the chip. It should be observed that the plastic deformation caused by a carbide is more than four orders of magnitude greater than the extra wear it causes.
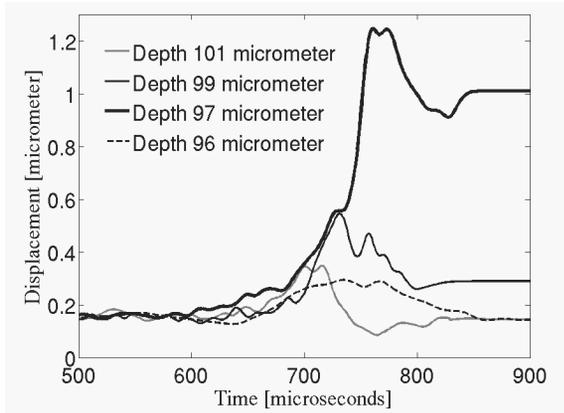
Fig. 11. Deformation measured in point A, see Figure 7, as a 10 µm carbide at different depth positions passes the tool
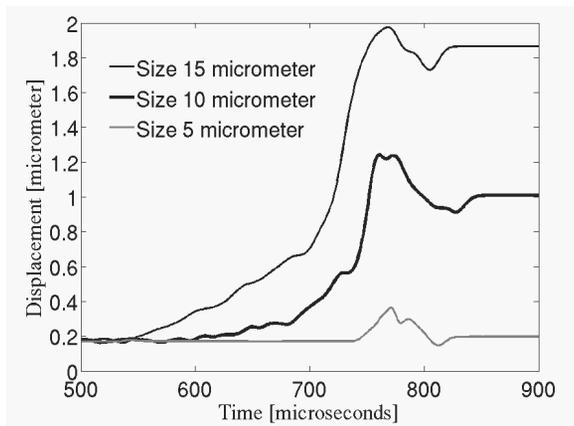
Fig. 12. Deformation measured in point A, see Figure 7, as a 10 µm carbide at different depth positions passes the tool

In Figure 12 tool wear is presented for point A of Figure 7 as a carbide with dimension of 5, 10 and 15 µm respectively, passes the tool tip. The dependence of tool tip plasticity on carbide size is highly non-linear, with a 15 µm particle causing about twice the plastic displacement of a 10 µm particle, while a 5 µm particle gives comparatively little plastic deflection, just 0.02 µm. Figure 13 shows plastic strains of about 40 times the elastic strains in the tip of the tool after a carbide with dimension 10 µm and start position 97 µm below the workpiece surface has passed.
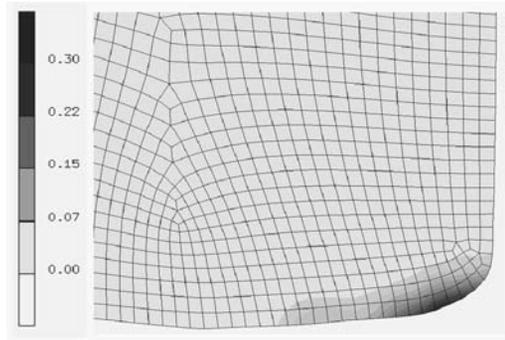
Fig. 13. Plastic deformation at the tool tip after the carbide with a dimension of 10 µm and start position of 97 µm below the workpiece surface has passed below the tool

4.2. Crater wear

Figure 14 shows the stresses in the tool as a quadratic carbide with a 10 µm dimension passes through the primary and secondary shear zones. The carbide's start position is 96 µm below the workpiece surface measured from the centre point of the carbide. As the carbide passes the shear zones, it rotates and the stress level in the tool increases, although still remaining below the yield limit of the tool. It can also be noted in this case, as well as for the case where the carbide passes below the tool tip, that it never comes in contact with the tool. Furthermore, it can be noted that, due to its high yield limit, the carbide does not deform plastically as it passes the through the shear zones.

Wear

In Figure 15 tool wear is presented for point B in Figure 7 as a carbide with dimension of 10 µm at different depth positions as it passes the tool tip. The tool wear is calculated using Usui's wear equation. The increase in tool wear is mainly due to an increase in pressure acting on the tool, while the temperature is constant and the relative velocity between the tool and the workpiece changes only slightly. The reason that, at a depth of 96 µm, the carbide is so much behind is due to the fact that it is delayed in a region at the beginning of the rake face close to the tool, where the chip moves extremely slowly as an effect of high normal stress resulting in large friction stress.

Plastic deformation

Figure 14 shows that the equivalent stress in the tool remains below the yield limit and consequently the tool does not deform plastically as the carbide passes by the rake face, a fact which

conforms to the generally-held opinion in the field of metal cutting that carbides mainly affect flank wear.

a)
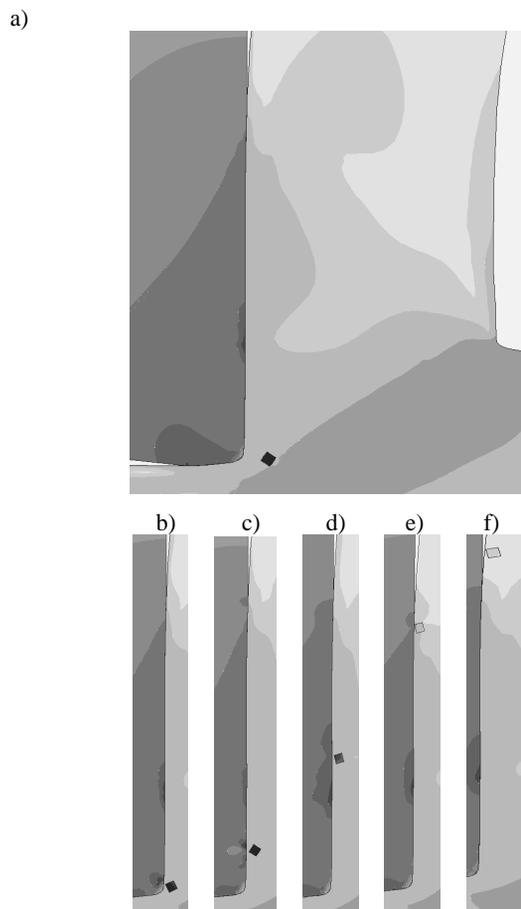
Fig. 14. Equivalent stresses in the tool as a carbide passes by the rake face at different times (measured from the start of the carbide collusion analysis, c.f. Figure 7), (a) 700 µs, (b) 800 µs, (c) 1100 µs, (d) 1400 µs , (e) 1800 µs, (f) 2000 µs. The size of the carbide is 10 µm and its start position is 96 µm below the workpiece surface measured from the centre point of the carbide
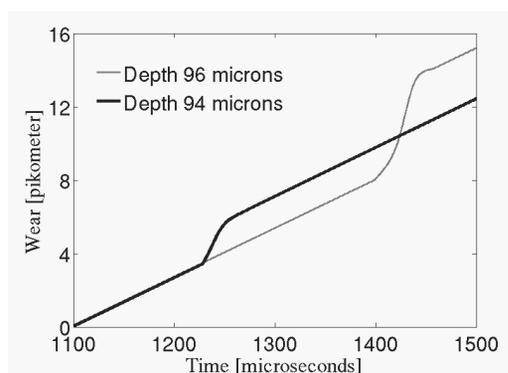
Fig. 15. Wear measured in point B, see Figure 7, as carbide at different depth position passing the rake face

5. Conclusions

The wear simulations performed reveal that embedded carbides may play a significant role in tool wear. However, contrary to intuition and the generally held opinion in the field of metal cutting the effect of particles on wear is not as a result of direct contact as a hard particle extends from the material and scratches the tool. The simulations show that hard particles remain shielded by surrounding softer material, and never in fact come into contact with the tool. Instead, they cause wear by increasing the local contact stress, even to the point of causing considerable plastic deformation. This could be an artefact in these specific simulations, but our conjecture is that it is a general physical effect that mandates further investigation.

A major conclusion to emerge from these preliminary calculations is that both the position, and in particular, the size of carbide particles, have a dramatic impact on the wear rate and plastic deformation in the tool. In particular, while small particles have negligible effect on wear rate and plastic deformation of the tool, particles larger than a certain size (about 5µm) cause plastic deformation of the tool tip when passing sufficiently close (within a few µm from the critical position). This plastic deformation is significant, of the order of one µm, and consequently critical for tool life. We conclude that the method presented provides a powerful tool for investigating the effect of microstructural features, such as hard carbides, on tool wear.

Acknowledgements

References

[1] N. Ahmed, A.V. Mitrofanov, V.I. Babitsky, V.V. Silberschmidt, Analysis of material response to ultrasonic vibration in turning Inconel 718, International Journal of Materials Science and Engineering 424 (2006) 318-325.

[2] E. Ceretti, P. Fallböhmer, W.T. Wu, T. Altan, Application of 2D FEM to chip formation in orthogonal cutting, Journal of Materials Processing Technology 59 (1996) 169-180.

[3] L. Chuzhoy, R.E. DeVor, S.G. Kapoor, D.J. Bammann, Microstructure-level modelling of ductile iron machining, Journal of Manufacturing Science and Engineering ASME 124 (2002) 162-169.

[4] L. Chuzhoy, R.E. DeVor, S.G. Kapoor, A.J. Beaudoin,. D.J. Bammann, Machining simulation of ductile iron and its constituents, part 1: Estimation of material model parameters and their validation, Journal of Manufacturing Science and Engineering ASME 125 (2003) 181-191.

[5] L. Chuzhoy, R.E. DeVor, S.G. Kapoor, Machining simulation of ductile iron and its constituents, part 2: Numerical simulation and experimental validation of

machining, Journal of Manufacturing Science and Engineering ASME 125 (2003) 192-201.

[6] N. Fang, A new quantitative sensitivity analysis of the flow stress of 18 engineering materials in machining, Proceedings of the ASME International Mechanical Engineering Congress "Manufacturing Engineering Division", Washington, 2003, vol. 14, 23-32.

[7] L .Filice, D. Umbrello, F. Micari, L. Setteneri, On the finite element simulation of thermal phenomena in machining process, Proceedings of the 8th Keynote International ESAFORM Conference, Cluj-Napoca, 2005, 729-732.

[8] L. Filice, F. Micari, L. Settineri, D. Umbrello, Wear modelling in mild steel orthogonal cutting when using uncoated carbide tools, Wear 262 (2007) 545-554.

[9] A.E. Focke, F.E. Westerman, J. Kemphaus, W.T. Shin, M. Hoch, Wear of superhard materials when cutting superalloys, Wear 46 (1978) 65-79.

[10] F. Klocke, H.W. Raedt, S. Hoppe, 2D-FEM Simulation of the orthogonal high speed cutting process, Machining Science and Technology 5/3 (2001) 323-340.

[11] T. Kitagawa, K. Maekawa, T. Shirakhashi, E. Usui, Analytical prediction of flank wear of carbide tools in turning plain carbon steels. Part 1. Characteristic equation of flank wear, Bulletin of the Japan Society of Precision Engineering 22/4 (1988) 263-269.

[12] T. Kitagawa, K. Maekawa, T. Shirakhashi, E. Usui, Analytical prediction of flank wear of carbide tools in turning plain carbon steels. Part 2. Prediction of flank wear, Bulletin of the Japan Society of Precision Engineering 23/2 (1989) 126-134.

[13] M. Krook, V. Recina, B. Karlsson, Material properties affecting the machinability of Inconel 718, Proceedings of the 6th International Special Emphasis Symposium "Superalloys 718, 625, 706 and Derivates", Pittsburgh, 2005, 613-627.

[14] J. Lorentzon, N. Järvstråt, Tool wear geometry updating in Inconel 718 turning simulations, Proceedings of the 9th CIRP International Workshop "Modeling of Machining Operations", Bled, 2006, 491-498.

[15] T. MacGinley, J. Monaghan, Modelling the orthogonal machining process using coated cemented carbide cutting tools, Journal of Materials Processing Technology 118 (2001) 293-300.

[16] K.E. Petersen, Silicon as a Mechanical Material, Proceedings of the IEEE 70/5 (1982) 420-457.

[17] R. Sievert, A.H. Hamann, D. Noack, P. Löwe, K.N. Singh, G. Künecke, Simulation of thermal softening, damage and chip segmentation in a nickel super-alloy, in: H.K. Tönshoff, F. Hollmann: Hochgeschwindigkeitspannen, Wiley-vch, 2005, 446-469.

[18] A. Simoneau, E. Ng, M.A. Elbestawi, Modelling the effects of microstructure in metal cutting, International Journal of Machine Tools and Manufacture 47 (2007) 368-375.

[19] E.M. Trent, Metal cutting, Butterwort, London, 2000.

[20] E. Usui, A. Hirota, M. Masuka, Analytical prediction of three dimensional cutting process. Part 3. Cutting temperature and crater wear of carbide tool, Journal of Engineering for Industry: Transactions of the ASME 100 (1978) 222-228.

[21] L.J. Xie, J. Schmidt, C. Schmidt, F. Biesinger, 2D FEM estimation of tool wear in turning operation, Journal of Materials Processing Technology 146 (2004) 82-91.

[22] Y.C. Yen, J. Anurag, T. Altan, A finite element analysis of orthogonal machining of different tool edge geometries, Journal of Materials Processing Technology 146 (2004) 72-81.

[23] Y.C. Yen, J. Söhner, B. Lilly, T. Altan, Estimation of tool wear in orthogonal cutting using the finite element analysis, Journal of Materials Processing Technology 146 (2004) 82-91.

[24] W.J. Zhang, B.V. Reddy, S.C. Deevi, Physical properties of TiAl-base alloys, Scripta Materialia 45 (2001) 645-651.

[25] CRC Material Science and Engineering handbook, 1994, ISBN 0-8493-4250-3.

[26] M. Johansson, V. Recina, B. Karlsson, Material properties affecting the machinability of Inconel 718, Proceedings of the 6th International Special Emphasis Symposium "Superalloys 718, 625, 706 and Derivates", Pittsburgh, 2005.